



HAL
open science

Synthesis of manganese oxide supported on mesoporous titanium oxide: Influence of the block copolymer

F. Schmit, L. Bois, R. Chiriach, F. Toche, Fernand Chassagneux, M. Besson, C. Descorme, L. Khrouz

► To cite this version:

F. Schmit, L. Bois, R. Chiriach, F. Toche, Fernand Chassagneux, et al.. Synthesis of manganese oxide supported on mesoporous titanium oxide: Influence of the block copolymer. *Journal of Solid State Chemistry*, 2015, 221, pp.291-301. 10.1016/j.jssc.2014.10.010 . hal-01149295

HAL Id: hal-01149295

<https://hal.science/hal-01149295>

Submitted on 8 Oct 2021

HAL is a multi-disciplinary open access archive for the deposit and dissemination of scientific research documents, whether they are published or not. The documents may come from teaching and research institutions in France or abroad, or from public or private research centers.

L'archive ouverte pluridisciplinaire **HAL**, est destinée au dépôt et à la diffusion de documents scientifiques de niveau recherche, publiés ou non, émanant des établissements d'enseignement et de recherche français ou étrangers, des laboratoires publics ou privés.



Distributed under a Creative Commons Attribution 4.0 International License

Synthesis of manganese oxide supported on mesoporous titanium oxide: Influence of the block copolymer

F. Schmit^{a,b}, L. Bois^{a,*}, R. Chiriac^a, F. Toche^a, F. Chassagneux^a, M. Besson^b, C. Descorme^b, L. Khrouz^c

^a Laboratoire des Multimatériaux et Interfaces, UMR CNRS 5615, Bât. Berthollet, Université Claude Bernard—Lyon 1, 43 Bd 11 novembre 1918, 69622 Villeurbanne, France

^b IRCELYON, Institut de recherches sur la catalyse et l'environnement de Lyon (UMR 5256 CNRS/Université Lyon 1), Lyon, France

^c ENS LYON Laboratoire de Chimie (LR6, site Monod), 46, allée d'Italie, 69364 Lyon Cedex 07, France

Manganese oxides supported on mesoporous titanium oxides were synthesized via a sol-gel route using block copolymer self-assembly. The oxides were characterized by X-ray diffraction, infrared spectroscopy, thermal analyses, nitrogen adsorption/desorption, electron microscopy and electronic paramagnetic resonance. A mesoporous anatase containing amorphous manganese oxide particles could be obtained with a 0.2 Mn:Ti molar ratio. At higher manganese loading (0.5 Mn:Ti molar ratio), segregation of crystalline manganese oxide occurred. The influence of block copolymer and manganese salt on the oxide structure was discussed. The evolution of the textural and structural characteristics of the materials upon hydrothermal treatment was also investigated.

1. Introduction

The development of active and stable solid catalysts for oxidation reactions in water at relatively high temperature and pressure is an important challenge, especially in the field of water treatment. As mesoporous oxides have a high specific surface area, high porous volume and pore size about 10 nm, they may have many advantages for the diffusion of molecules to be converted and so increase their interaction with the catalyst surface. Titania, used as a support, has been reported as stable under the reaction conditions of interest. Furthermore, transition metal oxides, including manganese oxide with many degrees of oxidation (+2, +3, +4, +7) were demonstrated to have interesting oxidation properties [1–5].

Manganese oxides have been extensively studied as catalysts in gas phase oxidation reactions [2,6–15] as well as in some selective reduction reactions [16–22]. They are also good candidates as catalysts in water treatment applications [23–25]. These oxides were evaluated in the catalytic wet air oxidation reaction when the elimination of organic pollutants occurs in the liquid phase using oxygen as the oxidant [3,26–31]. Another important application for manganese oxides is as electrode materials [32]. However, in this

article we focus our attention on the one pot synthesis of manganese oxides supported on mesoporous titania.

Manganese oxides are conventionally obtained either by oxidation of manganese(II) salts by KMnO_4 or by reduction of KMnO_4 by organic reagents [4]. Such oxides are often very porous but demonstrate limited thermal stability under the reaction conditions of interest. New synthetic methods have been developed for the elaboration of better nano-structured manganese oxides. One approach to synthesize nano-structured manganese oxides is the block copolymer self-assembly method, which has often been implemented with the objective of producing mesoporous oxides. This methodology is used to obtain oxides with high specific surface areas and well-defined porous structures. In fact, block copolymers form micelles with a hydrophobic core (consisting of polypropylene oxide chains) and a hydrophilic shell (consisting of polyethylene oxide chains). Single oxides may crystallize around these micelle assemblies. The polymer elimination leads to an oxide with a high mesoporosity. Using such a process, MnO_2 can be obtained with a specific surface area around $200 \text{ m}^2 \text{ g}^{-1}$ [13,33–42]. A mesoporous titania could also be easily prepared using the same procedure [43]. However, among the studies devoted to the elaboration of binary Mn–Ti oxides [44–50], very few reported the use of the self-assembly method [44]. Solid solutions of Mn in anatase were often reported [49–52], but binary oxides such as Mn_2TiO_4 and MnTiO_3 were also observed at high temperature [51–53]. For such bimetallic systems, the relative

* Corresponding author.

E-mail address: laurence.bois@univ-lyon1.fr (L. Bois).

localization of the two components is always a matter of discussion. Stoichiometric binary oxides, solid solutions or mixtures of simple oxides are obtained. From the catalytic application point of view, the accessibility of the active phase is the key point.

In this paper, we describe the synthesis of mixed manganese and titanium oxides using the self-assembly process with a polyethylene oxide–polypropylene oxide block copolymer. Our attention focuses on the influence on the material structure of (i) the presence of the block copolymer and (ii) the nature of the manganese salt used as the precursor. Block copolymers have been shown to form complexes with metal cations [54–56]. Manganese oxide could be introduced either inside the titania walls or at the titania surface by choosing a good manganese precursor having more or less affinity either with the polymer and/or with the titania sol.

2. Experimental

2.1. Synthesis of the materials

The titania gels were prepared following the method described by Ismail et al. [57]. $\text{Ti}(\text{OBu})_4$ (3.4 g, 10^{-2} mol) in ethanol (25 mL) was mixed with 1.6 g of Pluronic[®] F-127, a polyethylene oxide–polypropylene oxide (PEO₁₀₆–PPO₇₀–PEO₁₀₆—herein referred to as P) block polymer, 2.3 mL of acetic acid and 0.74 mL of hydrochloric acid (37 wt%). Manganese was incorporated in the titania sol in various proportions using $\text{MnCl}_2 \cdot 4\text{H}_2\text{O}$ or $\text{Mn}(\text{acetylacetonate})_2$ (referred to as $\text{Mn}(\text{acac})_2$). The Mn:Ti molar ratio was fixed at 0.2 or 0.5. Colourless sols were rapidly obtained when the $\text{MnCl}_2 \cdot 4\text{H}_2\text{O}$ salt was used, while a yellow sol formed more slowly with $\text{Mn}(\text{acac})_2$. The sols were slowly evaporated until formation of a gel. The samples were thermally treated at 450 °C for 5 h (temperature ramp of 1 °C min⁻¹), and black powders were obtained. Finally, in order to assess their hydrothermal stability, the samples (80 mg) were put inside a 250 mL autoclave at 200 °C for 24 h. Brown powders were systematically obtained after such hydrothermal treatment.

In the $\text{TM}_{xy}P_z$ samples, the subscripts x , y , z and h refer to the following:

- x indicates the nature of the manganese salt (Cl for $\text{MnCl}_2 \cdot 4\text{H}_2\text{O}$ and A for $\text{Mn}(\text{acac})_2$). x is omitted when the solid did not contain manganese.
- y indicates the theoretical Mn:Ti molar ratio. y is 0 when the solid did not contain any manganese.
- z indicates the amount of block copolymer introduced in the preparation ((0) 0 g, (1) 0.8 g, (2) 1.6 g, (3) 3.2 g). z is omitted whenever the solid contained a 1.6 g polymer proportion.
- Finally, if the sample had been hydrothermally treated, an h is introduced at the end of the sample reference (e.g. $\text{TM}_{xy}P-h$).

2.2. Characterization

X-ray diffraction (XRD) patterns were recorded on a PANalytical Xpert Pro diffractometer equipped with a monochromator, using $\text{CuK}\alpha$ radiation (1.54 Å). The sample texture was also analyzed via nitrogen adsorption/desorption using a Sorptomatic 1990 (CE Instruments, Milan, Italy). Prior to analysis, the samples were degassed under vacuum at 70 °C for 4 h.

The specific surface area was determined using the Brunauer–Emmett–Teller (BET) method. The average pore size (d_{mean}) and the mesoporous volume were calculated from the adsorption curve of the isotherm using the Barrett–Joyner–Halenda (BJH)

method. FTIR spectra were recorded on a SAFAS instrument using KBr pellets.

Thermogravimetric analyses with a simultaneous differential thermal analysis signal were performed on a TGA/SDTA Mettler Toledo 851 apparatus. The sample (20 mg) was introduced in an aluminum crucible and the temperature was increased to 500 °C at 10 °C min⁻¹. Air was used as the reactive gas (50 mL min⁻¹). For $\text{TM}_{x0.2}P$ and $\text{TM}_{x0.2}P_0$, the temperature was increased to 1200 °C at 20 °C min⁻¹. Relatively broad signals were obtained due to the high heating rate.

DSC analyses were performed on a DSC1 Mettler-Toledo apparatus. The solid to be analyzed (ca. 10 mg) was placed in a 40 μL aluminum pan, with a pierced lid and sealed before introduction into the DSC cell. Each analysis consisted of two steps. First, the temperature was increased to 500 °C (10 °C min⁻¹) before cooling down to room temperature. Then, air was used as the reactive gas (30 mL min⁻¹). Additional DSC experiments were also performed up to 700 °C (20 °C min⁻¹) on the $\text{TM}_{xy}P$ samples. SEM images were acquired on an S800 Hitachi microscope operated at 15 kV.

TEM images were obtained on a Topcon instrument operated at 200 kV. Before observation, the samples were ground and deposited on a copper grid covered with a holey carbon film.

EPR experiments on the $\text{TM}_{\text{Cl}0.2}P$ sample were done using an X-band spectrometer (Bruker EMX plus, double mode) and an X-band (9.4 GHz) Bruker ESP 500E spectrometer using a standard rectangular cavity. Simulation of the spectra was realized with “easyspin” (Matlab toolbox). The experimental spectra were simulated using the following parameters: frequency, 9.64 GHz; temperature, 70 K; microwave power, 6.41 mW; amplitude modulation 5 G; and modulation frequency, 100 kHz.

3. Results

3.1. XRD results

The $\text{TM}_{x0.2}P$ samples with the lowest Mn:Ti ratio (0.2) and synthesized in the presence of a medium proportion (1.6 g) of block copolymer, were characterized by XRD (Fig. 1a). The XRD pattern of the reference sample prepared without addition of any manganese salt (TM_0P) was characteristic of the anatase phase of TiO_2 (ICDD no. 01-084-1285). Upon addition of manganese ($\text{TM}_{\text{Cl}0.2}P$ and $\text{TM}_{\text{A}0.2}P$), the diffraction patterns showed a less crystalline anatase TiO_2 phase, with a shift of the (0 0 4) reflection line towards higher diffraction angles (see insert on Fig. 1a). Such a shift had already been seen in the case of the Mn–Ti–O system and attributed to the substitution of Mn^{4+} (ionic radius 0.67 Å) for Ti^{4+} (ionic radius 0.68 Å) [49–50]. Furthermore, the (1 0 5) and (2 1 1) reflections initially observed at 53.9° and 55.0°, respectively, merged. Finally, no crystallization of any manganese oxide was detected.

To determine the influence of the presence of the block copolymer on the synthesis, reference samples ($\text{TM}_{x0.2}P_0$) synthesized without addition of any block copolymer were studied (Fig. 1b). When no manganese was added to the preparation (TM_0P_0), the diffraction pattern was characteristic of the anatase phase (A, ICDD no. 01-084-1285) as in the case of the TM_0P sample when a medium proportion of block copolymer was used. However, a higher degree of crystallization was observed. When the $\text{MnCl}_2 \cdot 4\text{H}_2\text{O}$ precursor was used ($\text{TM}_{\text{Cl}0.2}P_0$), the diffraction pattern showed the formation of a very well crystallized Mn_2O_3 bixbyite phase (bx, ICDD 01-089-2809), while crystallization of the TiO_2 anatase phase decreased in comparison with the solids synthesized in the presence of Pluronic[®] F-127, with the same Mn precursor. In the presence of the $\text{Mn}(\text{acac})_2$ precursor ($\text{TM}_{\text{A}0.2}P_0$),

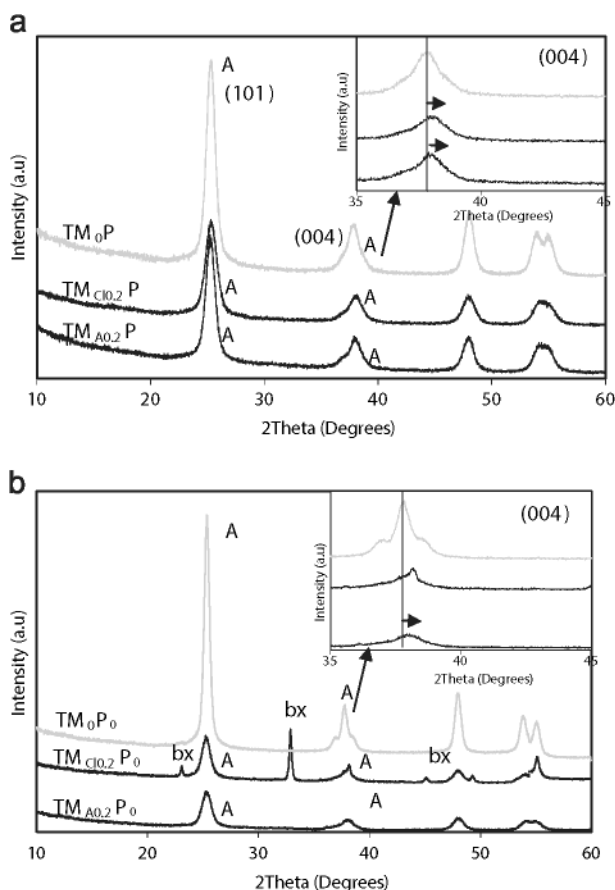


Fig. 1. X-ray diffraction patterns of $TM_{x0.2}P$ (a) and $TM_{x0.2}P_0$ (b) samples. A: anatase, bx: bixbyite.

the anatase phase was the only one detected. However, a shift of the (0 0 4) diffraction line was observed.

In the second step, samples with a higher Mn:Ti ratio (0.5) were (i) synthesized using the medium block copolymer ratio ($TM_{x0.5}P$) and (ii) analyzed by XRD (Fig. 2a). When the $MnCl_2 \cdot 4H_2O$ precursor was used ($TM_{Cl0.5}P$), the XRD characterization revealed the presence of the anatase TiO_2 phase together with the bixbyite Mn_2O_3 (bx), and the Mn_5O_8 manganese oxide phases (m, ICDD no. 00-39-1218). With the $Mn(acac)_2$ precursor ($TM_{A0.5}P$), the anatase crystallization drastically decreased. In turn, low crystalline rutile (R, ICDD no. 01-089-4920) and brookite phases (B, ICDD no. 01-076-1934) appeared. In addition, a MnO_2 ramsdellite phase (q, ICDD no. 00-042-1316) was detected.

To assess the influence of the block polymer on the $MnCl_2 \cdot 4H_2O$ precursor dispersion, the amount of Pluronic® F-127 was varied (Fig. 2b). With the highest block copolymer proportion ($TM_{Cl0.5}P_h$), the bixbyite phase appeared to be poorly crystalline (by XRD analysis), while traces of a new Mn_5O_8 phase (m) were detected. On the contrary, with the lowest block copolymer proportion ($TM_{Cl0.5}P_l$), the bixbyite phase reflection line at 33.0° became more intense. In fact, the higher the block copolymer concentration, the more difficult the manganese oxide phase crystallization. The anatase phase crystallization state was also reduced.

To summarize the different XRD observations, we can say that:

- whatever the precursor, some of the manganese ions could substitute for the titanium ions and also insert into the anatase lattice, as revealed by the shift of the (0 0 4) reflection line.
- the block copolymer allowed the dispersion of the $MnCl_2 \cdot 4H_2O$ salt even at the 0.2 Mn:Ti ratio. In the absence of the block

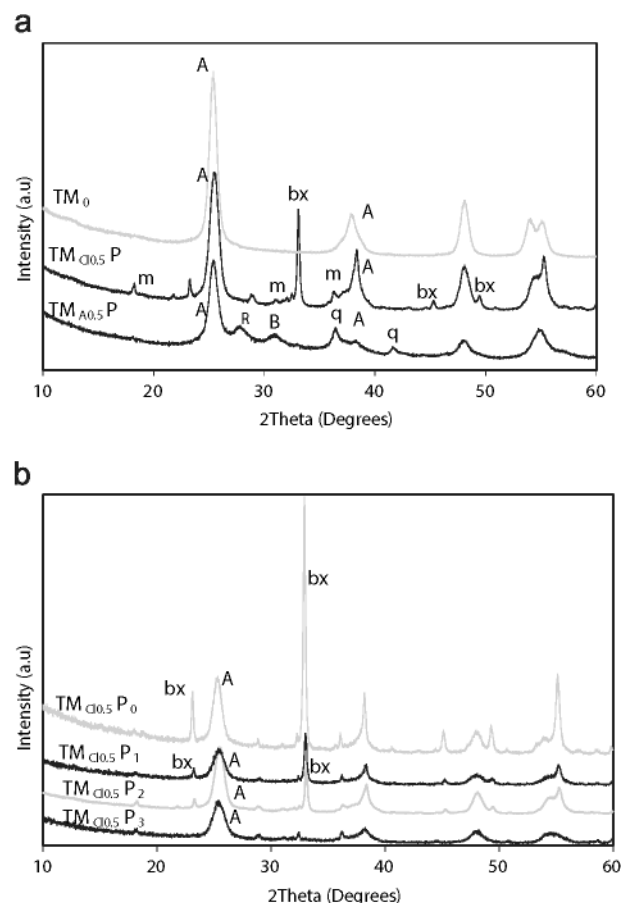


Fig. 2. (a) XRD patterns of the $TM_{x0.5}P$ samples. A: anatase, R: rutile, B: brookite, bx: bixbyite, m: Mn_5O_8 , q: MnO_2 (ramsdellite). (b) XRD patterns of the $TM_{Cl0.5}P_z$ samples with different polymer/Ti ratios.

copolymer, manganese mostly crystallized outside the titania network as a bixbyite phase (Mn_2O_3).

- the block copolymer delayed anatase crystallization.
- the $Mn(acac)_2$ precursor was dispersed in the titanium oxide even without the block copolymer and no manganese oxide crystallization was observed.

3.2. FTIR

The FTIR spectra of $TM_{x0.2}P$ and $TM_{x0.2}P_0$ samples showed a broad vibration band between 500 and 700 cm^{-1} (Fig. 3), except for the $TM_{Cl0.2}P_0$ sample, where well-defined vibration bands appeared at 655 , 600 , 570 , 520 and 500 cm^{-1} . The latter are characteristic of the Mn_2O_3 bixbyite phase [60]. In agreement with the XRD results, these observations confirmed that (i) the crystallization of the Mn_2O_3 phase occurred when the $MnCl_2 \cdot 4H_2O$ precursor was used, (ii) the crystallization of manganese oxide did not occur when $Mn(acac)_2$ was used and (iii) the crystallization of the Mn_2O_3 phase was delayed in the presence of the block copolymer.

3.3. Thermal analyses

In order to better understand the interaction between the manganese salts and the block copolymer, thermal analyses were performed. DSC and TGA/SDTA experiments were carried out on the pure manganese salts, the pure block copolymer and mixtures of the different manganese salts with the block copolymer (1 g of

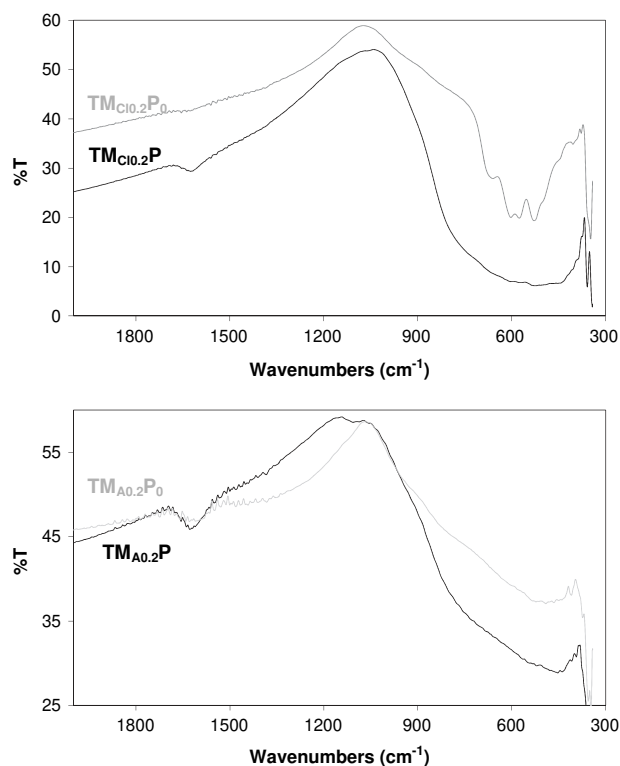


Fig. 3. FTIR spectra of the $TM_{x0.2}P$ and $TM_{x0.2}P_0$ samples.

manganese salt for 2 g of polymer). Mixtures were dissolved in ethanol before drying in order to observe the melting behaviour.

DSC thermograms of the pure compounds are given in Fig. 4a. For the block copolymer alone, two signals appeared. The first was an endothermic peak ca. 55 °C, characteristic of the polymer melting; while the second starting from 150 °C was due to the exothermic degradation of the polymer. The thermogram of the $MnCl_2 \cdot 4H_2O$ salt showed three endothermic peaks, with onset temperatures at 58 °C, 110 °C and 170 °C, corresponding to one melting and two dehydration steps, respectively. In turn, for the $Mn(acac)_2$ salt, a multi-step exothermic signal starting from 213 °C was observed. This was attributed to the degradation of the salt.

For the mixture of Pluronic® F-127 and $MnCl_2 \cdot 4H_2O$ (Fig. 4b), the degradation process was characterized by a single exothermic signal starting at 160 °C. The signals characteristic of the block copolymer alone and the manganese salt alone completely disappeared. The thermogram of the mixture of $Mn(acac)_2$ and the block copolymer showed both an endothermic process at 55 °C and an exothermic one ca. 190 °C. For the latter, the polymer melting temperature was unchanged in the presence of the salt, but the melting enthalpy of the polymer in the mixture compared to the polymer alone decreased by 10%, compared to the polymer alone. We hypothesized that this decrease was due to the interaction of part of the polymer (ca. 10%) with the manganese precursor. Furthermore, the degradation temperature of the mixture was systematically higher compared to the degradation temperature of the polymer alone.

To sum up, the DSC analyses showed that polymer melting was no longer observed when the polymer was mixed with $MnCl_2 \cdot 4H_2O$. However, the melting phenomenon was still partly preserved in the presence of $Mn(acac)_2$. This indicated that the polymer acts as a ligand for the Mn^{2+} ions in $MnCl_2 \cdot 4H_2O$ salt, while the complexation is much weaker with $Mn(acac)_2$. In the polymer-salt mixtures, the degradation temperatures were modified

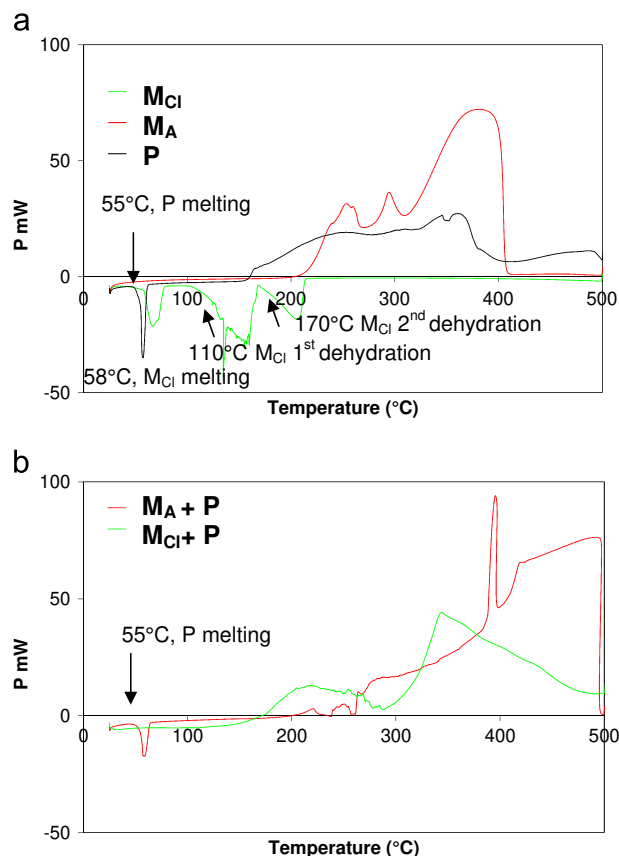


Fig. 4. DSC analyses of the pure manganese salts and the manganese salt-block copolymer mixtures.

compared to the pure compounds and appeared to be delayed in the case of $Mn(acac)_2$ [61].

TGA with simultaneous differential thermal analysis (TGA-SDTA) was also done to investigate the decomposition processes in more detail (Fig. 5). We found that for the pure $MnCl_2 \cdot 4H_2O$ salt, the SDTA profile (Fig. 5b) showed an endothermic reaction around 60 °C, which could be attributed to the melting process since there was no associated loss of mass (Fig. 5a). The two subsequent endothermic SDTA signals at 150 and 210 °C were assigned to the two major dehydration processes leading to $MnCl_2$ (identified by XRD) as observed on the TGA curve (3 and 1 mol of H_2O were lost respectively upon these two dehydration steps).

In the case of $Mn(acac)_2$, the SDTA did not show any endothermic reaction. However, an exothermic reaction starting ca. 210 °C was attributed to the degradation process (Fig. 5b). This was in agreement with the TGA analysis (Fig. 5a) and the loss of mass observed from this temperature and above. In fact, the degradation process was incomplete at 500 °C and led to a mixture of Mn_5O_8 and Mn_2O_3 (identified with XRD).

For the block copolymer, the negative signal at about 50 °C (Fig. 5b) was attributed to melting since there was no associated loss of mass observed during the simultaneous TGA analysis (Fig. 5a). The degradation was characterized by the exothermic reaction between 200 and 400 °C and confirmed by TGA. Degradation of the polymer was found to be complete by 500 °C.

For the mixture of the polymer with $MnCl_2 \cdot 4H_2O$ (Fig. 5d), no signal could be attributed to any melting or dehydration phenomena. This was confirmed by the TGA results where the mass loss attributed to degradation started at a higher temperature compared to the pure polymer (Fig. 5c). However, melting was still detectable in the case of the polymer $Mn(acac)_2$ mixture (Fig. 5d). However, the degradation

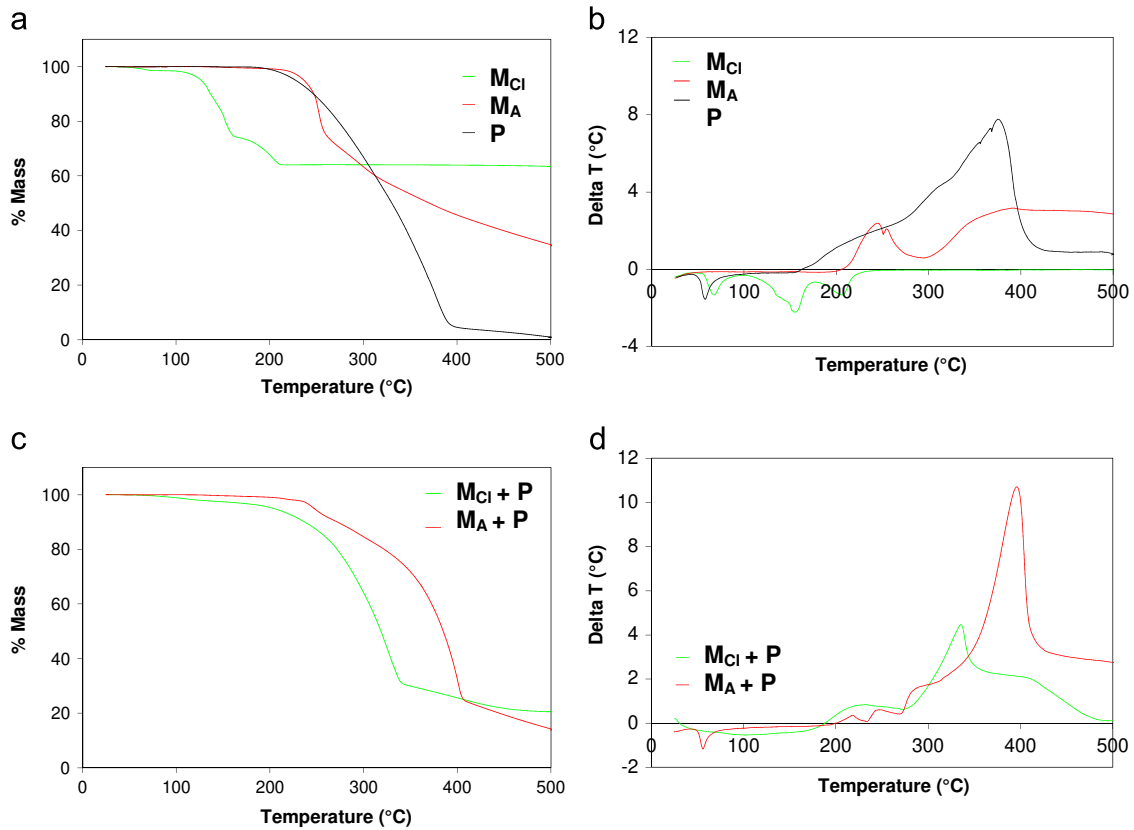


Fig. 5. TGA and SDTA analyses of the pure manganese salts and the manganese salt-block copolymer mixtures.

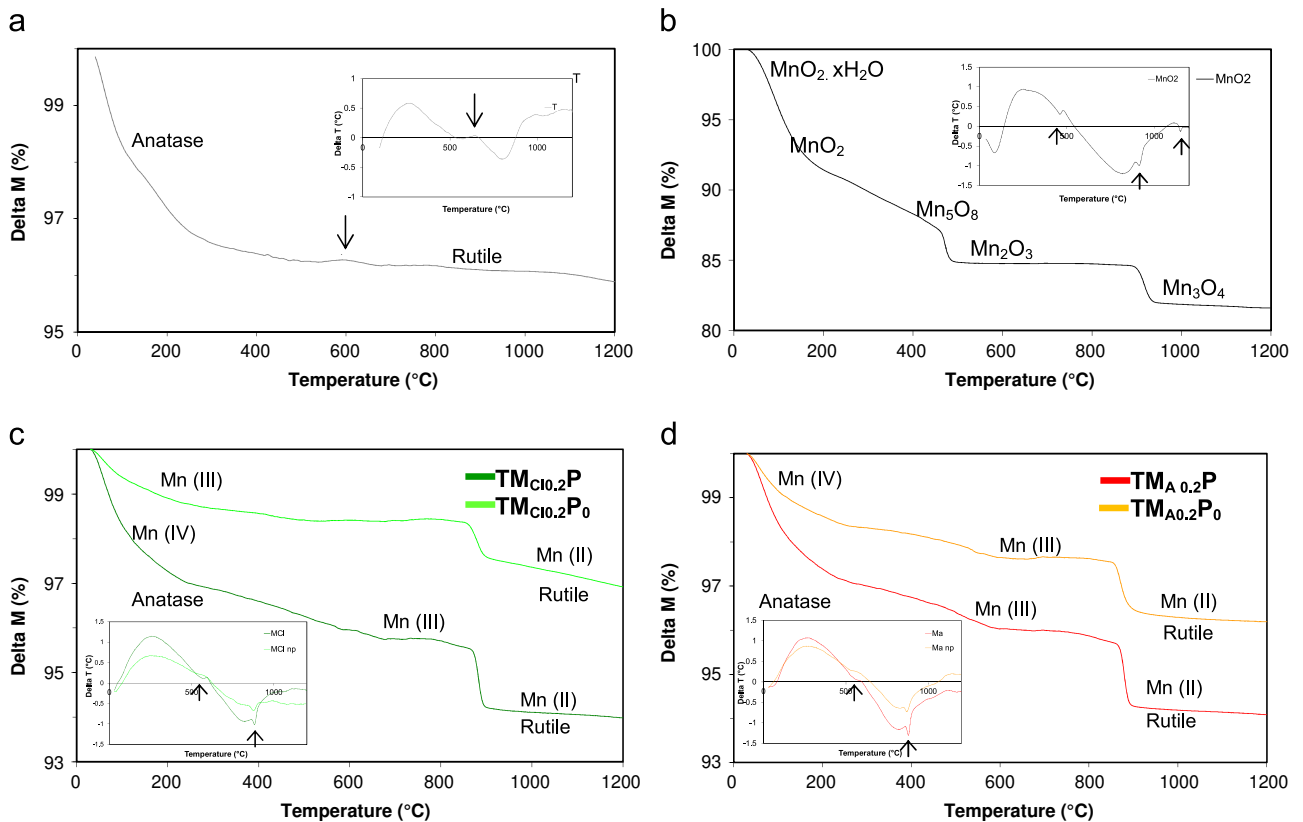


Fig. 6. DSC analyses of the $TM_{x,0.2}P$ and $TM_{x,0.2}P_0$ samples.

process was also delayed at higher temperatures compared to the pure polymer, as in the previous case. Therefore, SDTA and TGA results confirmed the previous observations derived from the DSC analyses.

To follow the evolution of the degree of manganese oxidation upon heating, TGA-SDTA was also performed on different samples as well as on reference TiO_2 and MnO_2 samples after thermal treatment at 450°C under air (Fig. 6). We observed that the transformation of the anatase phase to rutile was characterized by a small exothermic transition at 650°C [62] (Fig. 6a). The MnO_2 sample analysis showed (i) a dehydration step associated with the first weight loss; (ii) a second weight loss attributed to the reduction of MnO_2 to a formula close to Mn_5O_8 (Fig. 6b); (iii) a third weight loss, associated with an endothermic peak around 450°C corresponding to the formation of Mn_2O_3 ; (iv) a fourth weight loss, also associated with an endothermic phenomenon at around 900°C , related to the subsequent reduction of Mn_2O_3 to Mn_3O_4 and (v) a final endothermic transition at 1170°C attributed to the transformation from $\alpha\text{-Mn}_3\text{O}_4$ to $\beta\text{-Mn}_3\text{O}_4$.

In the case of the two $\text{TM}_{\text{Cl}0.2}\text{P}$ and $\text{TM}_{\text{A}0.2}\text{P}$ samples, an initial weight loss around 100°C was observed (Fig. 6c and d). This was attributed to water desorption from the pores due to the presence of the polymer, as in the case of the TiO_2 sample (Fig. 6a). The second endothermic weight loss ($200\text{--}600^\circ\text{C}$) was attributed to the transformation of Mn(IV) species into Mn(III) (Mn_2O_3). This second transition was barely observed in the case of the $\text{TM}_{\text{Cl}0.2}\text{P}_0$ sample, i.e. in the absence of polymer. A third weight loss also occurred at 900°C for all samples, due to the transformation of some Mn(III) into Mn(II) species, upon crystallization of the MnTiO_3 and TiO_2 rutile phases. The latter reduction steps from Mn(IV) to Mn(III) and from Mn(III) to Mn(II) were more pronounced when the polymer was present. Similarly, when the block copolymer was used, a better agreement was found between the experimental and theoretical losses (1.6%, Table 1). In these samples, manganese species were mainly present as Mn(IV), either included in a solid solution or as very well-dispersed amorphous MnO_2 . At 900°C , the conversion into MnTiO_3 was rapid and complete. On the contrary, when no polymer was used in the synthesis, a large proportion of the manganese was present as Mn(III), with a lower reactivity upon transformation into MnTiO_3 . The TGA results proved that one of the major effects of the polymer was the stabilization of the Mn(IV) species, especially in the case of the $\text{MnCl}_2 \cdot 4\text{H}_2\text{O}$ salt.

3.4. Textural analyses

The textural properties of the $\text{TM}_{\text{x}0.2}\text{P}$ samples were characterized via nitrogen adsorption/desorption at liquid nitrogen temperature (Fig. 7). The results are summarized in Table 2. The isotherm of the pure titania TM_0P sample was type IV, according to the IUPAC classification [63] and characteristic of a mesoporous material. The H_2 -type hysteresis loop is common in mesoporous material having a complex pore structure (differing from cylindrical-like pores) [63]. The specific surface area was $140\text{ m}^2\text{ g}^{-1}$, pore volume $0.3\text{ cm}^3\text{ g}^{-1}$

Table 1
Comparison of calculated and experimental weight losses between 800°C and 1000°C .

	Mn precursor	Calculated wt loss (%)	Experimental wt loss (%)
$\text{TM}_{\text{Cl}0.2}\text{P}$	MnCl_2	1.60	1.6
$\text{TM}_{\text{Cl}0.2}\text{P}_0$	–	1.65	1.1
$\text{TM}_{\text{A}0.2}\text{P}$	$\text{Mn}(\text{acac})_2$	1.61	1.6
$\text{TM}_{\text{A}0.2}\text{P}_0$	–	1.63	1.4

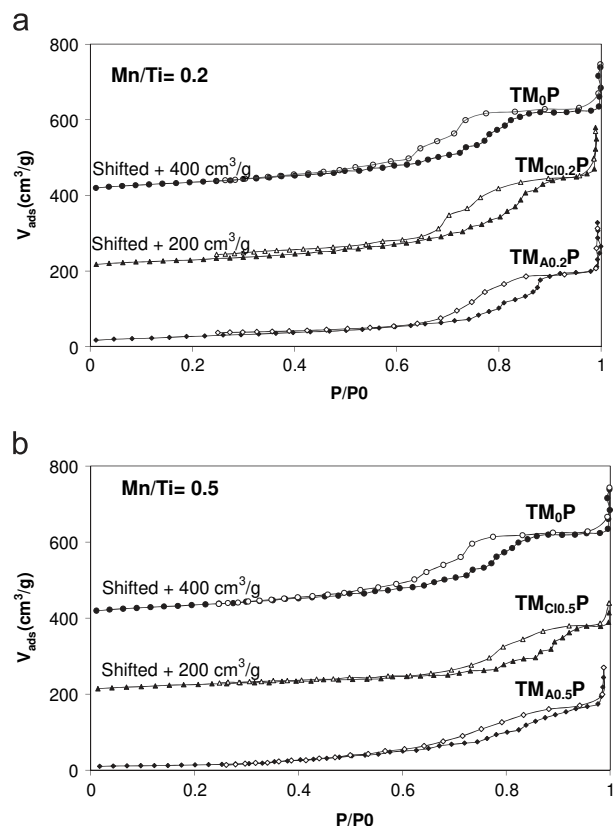


Fig. 7. Nitrogen adsorption/desorption isotherms of the $\text{TM}_{\text{xy}}\text{P}$ samples.

Table 2
Textural properties of $\text{TM}_{\text{xy}}\text{P}$, $\text{TM}_{\text{x}0.2}\text{P}_0$ and $\text{TM}_{\text{x}0.2}\text{P-h}$ samples.

	Mn:Ti	Mn precursor	Specific surface area ($\text{m}^2\text{ g}^{-1}$)	Pore volume ($\text{cm}^3\text{ g}^{-1}$)	Pore diameter (nm)
TM_0P	0	–	140	0.3	9
$\text{TM}_{\text{Cl}0.2}\text{P}$	0.2	MnCl_2	110	0.4	11
$\text{TM}_{\text{A}0.2}\text{P}$	0.2	$\text{Mn}(\text{acac})_2$	100	0.3	12
$\text{TM}_{\text{Cl}0.5}\text{P}$	0.5	MnCl_2	95	0.3	14
$\text{TM}_{\text{A}0.5}\text{P}$	0.5	$\text{Mn}(\text{acac})_2$	50	0.3	10
TM_0P_0	0	–	85	0.3	11
$\text{TM}_{\text{Cl}0.2}\text{P}_0$	0.2	MnCl_2	30	–	–
$\text{TM}_{\text{A}0.2}\text{P}_0$	0.2	$\text{Mn}(\text{acac})_2$	95	0.1	6
$\text{TM}_{\text{Cl}0.2}\text{P-h}$	0.2	MnCl_2	170	0.4	11
$\text{TM}_{\text{A}0.2}\text{P-h}$	0.2	$\text{Mn}(\text{acac})_2$	80	0.3	12

and pore diameter 9 nm. For the $\text{TM}_{\text{Cl}0.2}\text{P}$ and $\text{TM}_{\text{A}0.2}\text{P}$ samples, the isotherms were also type IV (Fig. 7a). However, compared to pure titania, the specific surface area slightly decreased while the pore size increased (ca. 11 nm). At higher manganese loading, i.e. at 0.5 Mn:Ti molar ratio ($\text{TM}_{\text{x}0.5}\text{P}$, Fig. 7b), isotherms are still type IV, but the specific surface areas were even smaller.

To test the impact of Pluronic[®] F127 on the textural properties of the different samples, a series of samples were synthesized in the absence of any block copolymer ($\text{TM}_{\text{x}0.2}\text{P}_0$, Table 2). For the pure titanium dioxide sample (TM_0P_0), a residual porosity was observed (specific surface area: $85\text{ m}^2\text{ g}^{-1}$, pore volume: $0.3\text{ cm}^3\text{ g}^{-1}$), probably due to the degradation of the organic part of the alkoxide precursor, behaving as a porogen agent [64]. For the mixed Mn–Ti oxides, the porosity collapsed completely in the case of manganese chloride salt ($\text{TM}_{\text{Cl}0.2}\text{P}_0$) which is coherent with the XRD results and the crystallization of a bixbyite phase. In the

case of the $\text{Mn}(\text{acac})_2$ precursor ($\text{TM}_{\text{A}0.2}\text{P}_0$), the specific surface area was maintained, while the pore volume and pore size decreased. Therefore, we can conclude that whatever the manganese precursor, the absence of block copolymer induced a decrease in the porosity, and this was much more pronounced with $\text{MnCl}_2 \cdot 4\text{H}_2\text{O}$.

3.5. TEM and SEM observations

TEM images of the samples prepared with the two different manganese precursors and a 0.2 Mn:Ti molar ratio are shown on Fig. 8. A disordered porosity was observed in all cases. It seems that mesopores are formed by the aggregation of nanoparticles. On the high resolution TEM micrographs for the $\text{TM}_{\text{Cl}0.2}\text{P}$ sample (Fig. 8c), some lattice fringes were seen with a spacing of 0.35 nm, which is the expected distance for the (1 0 1) planes of anatase (A). In addition, a very thin layer around the anatase crystallites was noted which could be related to the presence of an amorphous manganese oxide at the surface. For the $\text{TM}_{\text{A}0.2}\text{P}$ sample (Fig. 8d), no fringe characteristic of the (1 0 1) anatase planes was observed. However, fringes with 0.33 nm spacing were observed, as expected for the rutile (1 1 0) interplanar distance (R). Some fringes with 0.34 nm spacing were also detected. Such fringes have already been reported in the literature and are suggested as being characteristic of the modification of the anatase phase crystallization induced by the presence of manganese [19].

The SEM pictures of the $\text{TM}_{\text{x}0.2}\text{P}$, $\text{TM}_{\text{x}0.2}\text{P}_0$, $\text{TM}_{\text{x}0.5}\text{P}$ and $\text{TM}_{\text{x}0.5}\text{P}_0$ samples are shown on Fig. 9. In the absence of any block copolymer and with the $\text{MnCl}_2 \cdot 4\text{H}_2\text{O}$ salt, the manganese oxide phase segregation is clearly visible.

3.6. EPR characterization

In order to obtain more information on the manganese oxidation state, EPR characterizations were done on the $\text{TM}_{\text{Cl}0.2}\text{P}$ sample (not a new paragraph). The evolution of the resonance peaks as a function of temperature is shown on Fig. 10a. Two major peaks (resonances) are clearly observed at $T=70$ K. The broader one was attributed to Mn(IV) species with strong interactions between them, i.e. Mn in a cluster type environment [65–68]. In turn, the narrower peak was attributed to isolated Mn(IV), localized at the outer surface of the TiO_2 support. Furthermore, the hyperfine structure of the latter resonance peak observed at room temperature ($a_{\text{av}} \sim 95$ G, $g_{\text{av}} \sim 2$, Fig. 10a) was characteristic of the insertion of some Mn(II) ions inside the distorted TiO_2 anatase lattice [46,67]. However, both the fast disappearance of these two major components in perpendicular mode at high temperature (Fig. 10a) and the presence of a resonance peak at $g \sim 4$, in parallel mode (Fig. 10b), would indicate the predominance of Mn(IV) ions.

The EPR spectrum acquired at 70 K in perpendicular mode (Fig. 10c) was simulated using the following parameters:

- $S=3/2$, $g=[2.18, 1.95, 1.83]$, $D=0.0433 \text{ cm}^{-1}$, $E/D=0.33$, for isolated Mn(IV) ions;
- $S=1/2$ (intermediate spin state of Mn(IV)), $g=[1.97, 1.96, 1.95]$ for Mn in clusters.

The results were used to estimate the proportion of the different manganese species (Fig. 10d): 70% of the Mn(IV) ions were shown to be in a cluster-type environment and 30% as isolated Mn(IV) ions covering the titania surface.

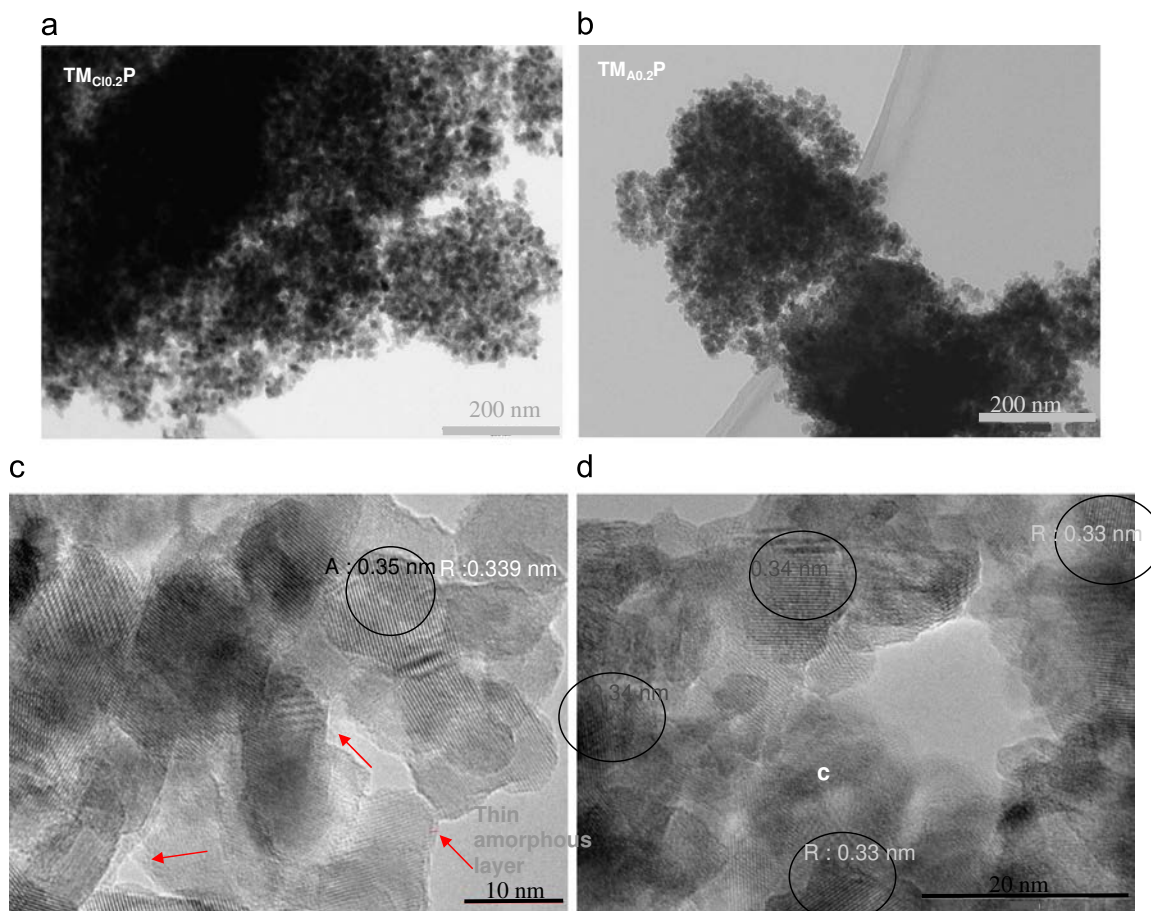


Fig. 8. TEM pictures of the $\text{TM}_{\text{x}0.2}\text{P}$ samples.

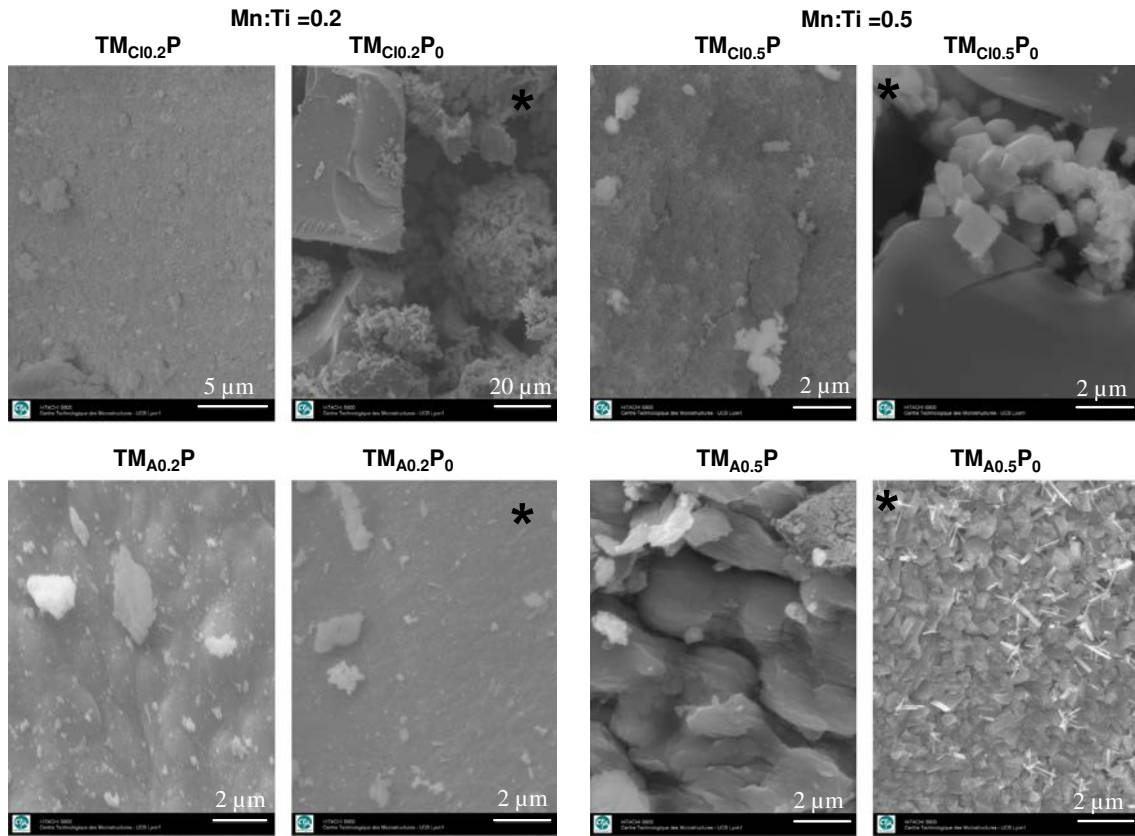


Fig. 9. SEM pictures of the $TM_{xy}P$ samples and TM_xP_0 samples.

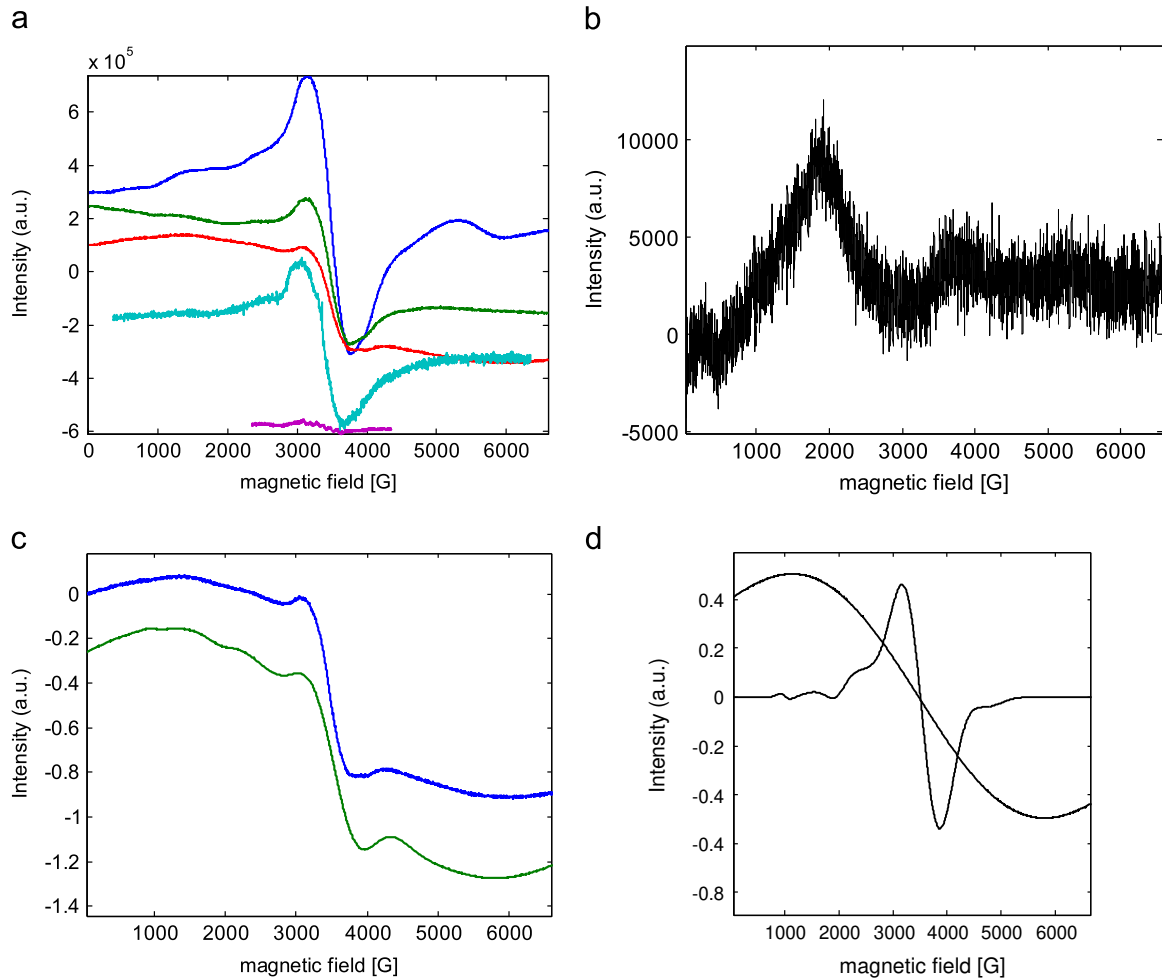


Fig. 10. EPR spectra of the $TM_{Cl0.2}P$ sample.

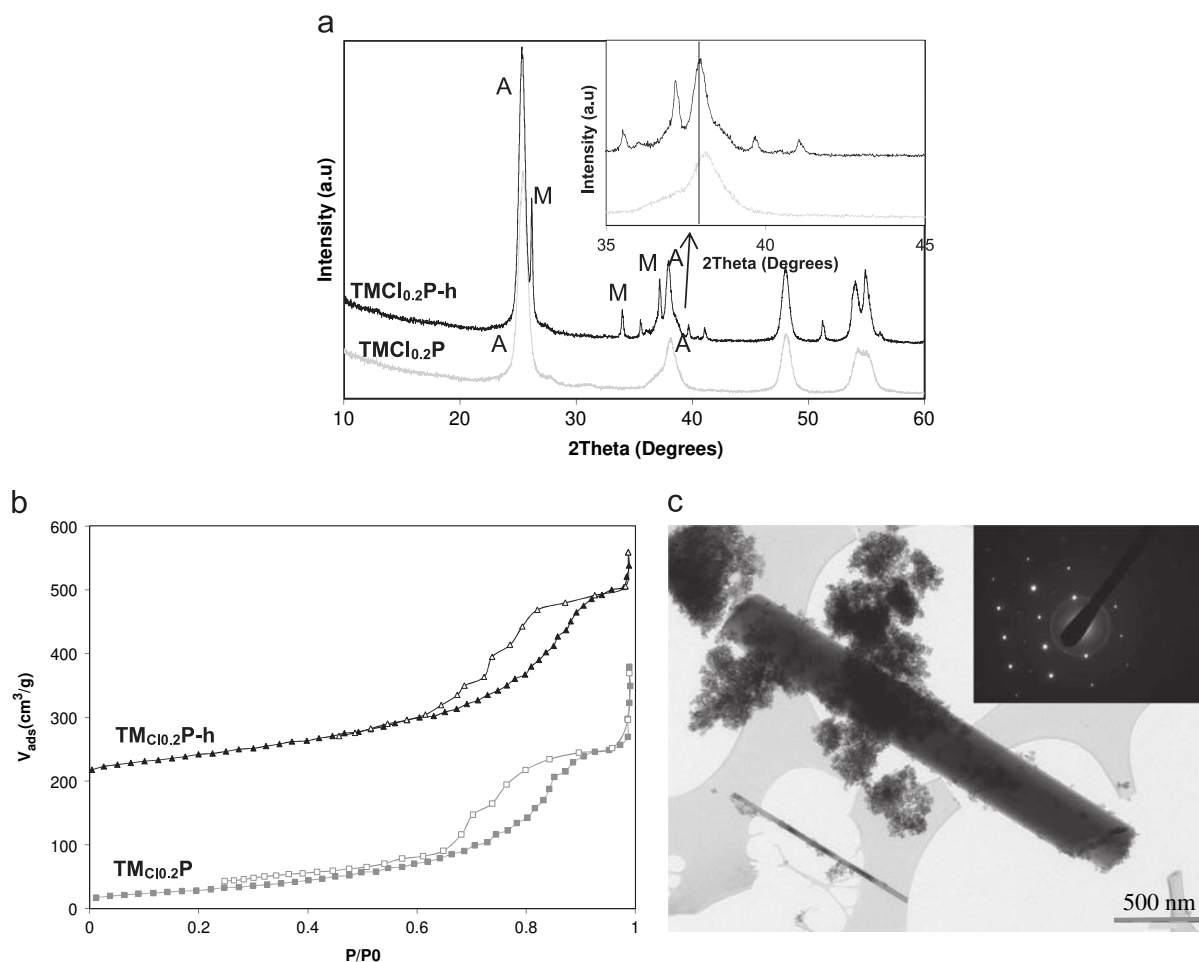


Fig. 11. (a) XRD patterns of the $\text{TM}_{\text{Cl}_{0.2}\text{P}}$ and $\text{TM}_{\text{Cl}_{0.2}\text{P-h}}$ samples before and after hydrothermal treatment. [M: MnOOH (manganite)]. (b) Nitrogen adsorption/desorption isotherms of the $\text{TM}_{\text{Cl}_{0.2}\text{P}}$ and $\text{TM}_{\text{Cl}_{0.2}\text{P-h}}$ samples. (c) TEM picture and electronic diffraction pattern of the sample $\text{TM}_{\text{Cl}_{0.2}\text{P-h}}$ after hydrothermal treatment.

In conclusion, these results revealed that:

- (i) most of the manganese (ca. 70%) was present as Mn(IV) in a cluster type environment, localized outside the titania crystals with strong interaction.
- (ii) some manganese (ca. 30%) was also present as Mn(IV) at the outer surface of the TiO_2 crystals, but with low interaction.
- (iii) only a very limited fraction of the manganese was localized inside the TiO_2 lattice in the form of Mn^{2+} . It is likely that Ti^{4+} had substituted for some Mn^{2+} , as already reported in the literature [58,59].

3.7. Hydrothermal stability

The hydrothermal stability of the mesoporous samples initially pre-treated at 450°C in dry air was then examined after further treatment in water at 200°C for 24 h (Fig. 11). XRD patterns (Fig. 11a) revealed some significant modifications of the crystalline structure of manganese oxide with the formation of a well crystallized MnOOH manganite phase (M, ICDD no. 041-1379). This observation is probably the same as the detection of manganese as manganite in natural waters [69]. Furthermore, the anatase phase was even more crystallized after hydrothermal treatment. The shift of the (0 0 4) reflection line toward lower angles can be explained by the expulsion of the manganese from the anatase lattice.

The textural properties of the solids were also shown to be slightly modified (Fig. 11b and Table 1) where the specific surface area increased for the $\text{MnCl}_2 \cdot 4\text{H}_2\text{O}$ precursor.

Finally, the TEM images and the associated electron diffraction patterns confirmed the high degree of crystallization of the manganese phase (Fig. 11c). The same evolution was observed for the two manganese precursors.

4. Discussion

The study of the influence of the block copolymer and manganese precursor during the one pot elaboration of manganese oxide supported on mesoporous titanium dioxides revealed several key points. First, the synthesized Mn–Ti–O solids exhibited a specific surface area ca. $100\text{ m}^2\text{ g}^{-1}$, a pore volume in the range of $0.3\text{--}0.4\text{ cm}^3\text{ g}^{-1}$ and an average pore size ca. 11 nm. In fact, the addition of manganese led to an increase in the average pore size from 9 to 11 nm, as reported earlier [44].

Second, the introduction of a manganese salt inside the titania-precursor sol modified the organization of this sol and led to a disordered mesoporous structure, where the anatase crystallization was lower and/or the manganese oxide crystallization was strongly delayed, compared to the pure phases. Combining the different characterization results, we conclude that manganese oxide is barely crystalline. Furthermore, the modifications induced by the manganese salt appeared to depend on the nature of the counter anion.

Third, no manganese oxide crystallization was observed at 0.2 Mn:Ti molar ratio, when $\text{MnCl}_2 \cdot 4\text{H}_2\text{O}$ precursor was used. This phenomenon had already been observed in previous work dealing with the synthesis of mixed Mn/Ti oxides via sol-gel with the incorporation of manganese into the anatase lattice [16,18,19,70–72]. Upon synthesis of a mesoporous Mn/Ti oxide, it was suggested that manganese oxide had covered the titania crystals as a result of the interactions between the Mn^{2+} cations and the block copolymer [44], and this hypothesis obviously applied in our study. In fact, the Mn_2O_3 bixbyite phase crystallization was further delayed as the proportion of block copolymer was increased. The block copolymer acted as a ligand for the Mn^{2+} cations forming some complexes and completely modifying the interactions with the titania-precursor sol. As a result, the localization of manganese oxide at the outer surface of the titania crystals was favoured. In turn, the mesoporous structure of the anatase phase was maintained. The possible formation of an amorphous MnO_2 shell covering the anatase crystals was confirmed by EPR with the evidence for two kinds of Mn(IV) populations: a cluster-type Mn(IV) and isolated Mn(IV).

We also showed that the block copolymer was essential to obtain a good dispersion of the manganese oxide phase with a very low crystallinity. The coordination of the Mn^{2+} cations and the polyethylene oxide entities on the block copolymer allowed a high degree of isolation of the manganese species and avoided crystallization of the manganese oxide phase. Previous studies had already shown the importance of these polyethylene oxide blocks on the dispersion of manganese inside a silica matrix [73–75]. In fact, transition metals are known to interact strongly with the hydrophilic part of the block copolymers and form complex micelles [54,56]. However, in the present study, we have demonstrated that the latter phenomenon is dependent on the nature of the manganese salt, due to different interactions between the salt and the block copolymer. The anatase structure was strongly modified when the $\text{Mn}(\text{acac})_2$ precursor was used. In fact, a mesoporous Mn–Ti–O “mixed” oxide probably formed and the block copolymer had no impact on the manganese localization. Acetylacetonate is known to chelate titanium, which strongly favours the formation of a solid solution between titanium and manganese.

Finally, further treatment of the solids under hydrothermal conditions modified the solid structure. The mesoporous titania structure was preserved but manganese was expelled from the mesoporous structure and crystallized as manganite (MnOOH) at the outer surface of the titania crystals. Therefore, if such mesoporous Mn–Ti–O mixed oxides were used in the catalytic wet air oxidation process, manganese would rapidly segregate outside the titania crystals as large manganite crystals.

5. Conclusion

Mesoporous manganese titanium oxides were successfully synthesized using a modified sol-gel process, involving a titanium alkoxide sol, manganese salt and block copolymer. The mesoporous oxides had a specific surface area ca. $100 \text{ m}^2 \text{ g}^{-1}$, pore volume of $0.3 \text{ cm}^3 \text{ g}^{-1}$ and 11 nm average pore size.

For a 0.2 Mn:Ti molar ratio with the $\text{MnCl}_2 \cdot 4\text{H}_2\text{O}$ precursor, the block copolymer strongly delayed the manganese oxide crystallization by chelating the Mn^{2+} cations leading to the formation of an amorphous layer around the anatase crystallites. In turn, with the $\text{Mn}(\text{acac})_2$ precursor, manganese species were highly dispersed inside the titania, even without any block copolymer. For a 0.5 Mn:Ti ratio, the Mn_2O_3 bixbyite (Mn(III)) or the MnO_2 ramsdellite (Mn(IV)) crystallized at the outer surface of the porous structure. Finally, upon hydrothermal treatment, manganese

crystallizes as manganite (MnOOH) at the surface of the titania support, while the titania mesostructure was preserved.

Acknowledgments

This work was financially supported by the Région Rhône-Alpes. The authors gratefully acknowledge the Région Rhône-Alpes for the Ph.D. grant awarded to France Schmit for the period 2011–2014.

The authors gratefully acknowledge Florian Molton and Carole Duboc, GHMFL-LCMI, Université Joseph Fourier Grenoble 1, for their help during the EPR experiments.

References

- [1] J.E. Post, Proc. Natl. Acad. Sci. U.S.A 96 (1999) 3447–3454.
- [2] X. Tang, J. Chen, X. Huang, Y. Xu, W. Shen, Appl. Catal., B: Environ 81 (2008) 115.
- [3] Z.Y. Ding, L. Li, D. Wade, E.F. Gloyna, Ind. Eng. Chem. Res. 37 (1998) 1707–1716.
- [4] S.L. Brock, N. Duan, Z.R. Tian, O. Giraldo, H. Zhou, S.L. Suib, Chem. Mater. 10 (1998) 2619–2628.
- [5] J.W. Dobereiner, J. Chem. Phys. 28 (1820) 223.
- [6] J. Quiroz Torres, S. Royer, J.P. Bellat, J.M. Giraudon, J.M. Lamonier, Chem-SusChem 6 (2013) 578–592.
- [7] M.A. Sidheswaran, H. Destailats, D.P. Sullivan, J. Larsen, W.J. Fisk, Appl. Catal., B: Environ 107 (17) (2011) 34–41.
- [8] Y. Sekine, Atmos. Environ. 36 (2002) 5543–5547.
- [9] F.N. Aguero, A. Scian, B.P. Barbero, L.E. Cadus, Catal. Today 133–135 (2008) 493–501.
- [10] Q. Ye, J. Zhao, F. Huo, D. Wang, S. Cheng, T. Kang, H. Dai, Microporous Mesoporous Mater. 172 (2013) 20–29.
- [11] F. Liu, S. Zuo, X. Xia, J. Sun, Y. Zou, L. Wang, C. Li, C. Qi, J. Mater. Chem. 1 (2013) 4089.
- [12] Y. Du, Q. Meng, J. Wang, J. Yan, H. fan, Y. Liu, H. Dai, Microporous Mesoporous Mater. 162 (2012) 199–206.
- [13] A.K. Sinha, K. Suzuki, M. Takahara, H. Azuma, T. Nonaka, K. Fukumoto, Angew. Chem. Int. Ed. 46 (2007) 2891–2894.
- [14] A.K. Sinha, K. Suzuki, M. Takahara, H. Azuma, T. Nonaka, N. Suzuki, N. Takahashi, J. Phys. Chem. C 112 (2008) 16028–16035.
- [15] T. Garcia, D. Sellick, F. Varela, I. Vazquez, A. Dejoz, S. Agouram, S.H. Taylor, B. Solsana, Appl. Catal., A—Gen 450 (2013) 169–177.
- [16] Y.J. Kim, H.J. Kwon, I.S. Nam, J.W. Choung, J.K. Kil, H.J. Kim, M.S. Cha, G.K. Yeo, Catal. Today 151 (2010) 244–250.
- [17] J. Li, J. Chen, R. Ke, C. Luo, J. Hao, Catal. Comm 8 (2007) 1896–1900.
- [18] Z. Wu, B. Jiang, Y. Liu, W. Zhao, B. Guan, J. Hazard. Mater 145 (2007) 488–494.
- [19] B. Jian, Y. Liu, Z. Wu, J. Hazard. Mater 162 (2009) 1249–1254.
- [20] M. Pourkhalil, A.Z. Moghaddam, A. Rashidi, J. Towfighi, K.J. Jozani, H. Bozorgzadeh, Catal. Lett. (2013) 184–192.
- [21] N. Tang, Y. Liu, H. Wang, Z. Wu, J. Phys. Chem. C 115 (2011) 8214–8220.
- [22] Z. Wu, N. Tang, L. Xiao, Y. Liu, H. Wang, J. Colloid Interface Sci 352 (2010) 143.
- [23] H.J. Ulrich, A.T. Stone, Environ. Sci. Technol 23 (1989) 421–428.
- [24] B. Nowack, A.T. Stone, J. Phys. Chem. B 106 (2002) 6227–6233.
- [25] C.S. Mc Ardell, A.T. Stone, J. Tian, Environ. Sci. Technol 32 (1998) (29323–29330).
- [26] J. Liu, C. Yu, P. Zhao, G. Chen, Appl. Surf. Sci 258 (2012) 9096.
- [27] F. Arena, C. Italiano, A. Raneri, C. Saja, Appl. Catal., B: Environ 99 (2010) 321–328.
- [28] L. Kong, W. Wei, Q. Zhao, J.Q. Wang, Y. Wan, ACS Catal 2 (2012) 2577–2586.
- [29] Y. Yao, C. Xu, S. Yu, D. Zhang, S. Wang, Ind. Eng. Chem. Res. 52 (2013) 3637–3645.
- [30] H. Liang, H. Sun, A. Patel, P. Shukla, Z.H. Zhu, S. Wang, Appl. Catal., B: Environ 127 (2012) 330–335.
- [31] X. Li, X. Lu, Y. Meng, C. Yao, Z. Chen, J. Alloys Compd. 562 (2013) 56–63.
- [32] W. Wei, X. Cui, W. Chen, D.G. Ivey, Chem. Soc. Rev. 40 (2011) 1697–1721.
- [33] J. Yuan, K. Lauberndts, Q. Zhang, S.L. Suib, J. Am. Chem. Soc. 125 (2003) 4966.
- [34] J. Luo, S.L. Suib, Chem. Commun. 11 (1997) 1031.
- [35] Z.R. Tian, W. Tong, J.Y. Wang, N.G. Duan, V.V. Krishnan, S.L. Suib, Science 276 (1997) 926.
- [36] Y. Zhang, Y. Yang, Y. Zhang, T. Zhang, M. Ye, Appl. Catal., B: Environ 127 (2012) 182–189.
- [37] F. Polzer, S. Wunder, Y. Lu, M. Ballauff, J. Catal. 289 (2012) 80–87.
- [38] Z. Zhao, J. Liu, F. Cui, H. Feng, L. Zhang, J. Mater. Chem. 22 (2012) 9052.
- [39] X. Xiao, S.P. Sun, M.B. Mc bride, A.T. Lemley, Environ. Sci. Pollut. Res. 20 (2013) 10–21.
- [40] R. Zhai, Y. Wan, L. Liu, X. Zhang, W. Wang, J. Liu, B. Zhang, Water Sci. Technol. 65 (2012) 1054.
- [41] F. Jiao, H. Frei, Energy Environ. Sci 3 (2010) 1018–1027.
- [42] M.M. Najafpour, A.N. Moghaddam, New. J. Chem. 36 (2012) 2514–2519.
- [43] K. Liu, M. Zhang, K. Shi, H. Fu, Mater. Lett. 59 (2005) 3308–3310.
- [44] M. Xue, L. Huang, J.Q. Wang, Y. Wang, L. Gao, J.H. Zhu, Z.G. Zou, Nanotechnol. 19 (2008) 185604.

- [45] E.A. Belaya, V.V. Viktorov, *Inorg. Mater* 44 (2008) 62–66.
- [46] R. Arroyo, G. Cordoba, J. Padilla, V.H. Lara, *Mater. Lett.* 54 (2002) 397–402.
- [47] M. Valigi, A. Cimino, *J. Solid State Chem* 12 (1975) 135–143.
- [48] M. Valigi, D. Cordischi, D. Gazzoli, V. Indovina, *J. Inorg. Nucl. Chem* 38 (1976) 1249–1253.
- [49] J.M. Gallardo-Amores, T. Armaroli, G. Ramis, E. Finocchio, G. Busca, *Appl. Catal., B: Environ* 22 (1999) 249–259.
- [50] J.P. Xu, J.F. Wang, Y.B. Lin, X.C. Liu, Z.L. Lu, L.Y. Lv, F.M. Zhang, Y.W. Du, *J. Phys. D: Appl. Phys* 40 (2007) 4757–4760.
- [51] Y.B. Kang, H.G. Lee, *ISIJ Int.* 11 (2005) 1543–1551.
- [52] J.P. Xu, S.B. Shi, L. Li, J.F. Wang, L.Y. Lv, F.M. Zhang, Y.W. Du, *J. Phys. Chem. Solids* 70 (2009) 511–515.
- [53] G.W. Zhou, Y.S. Kang, *Mater. Sci. Eng., C* 24 (2004) 71–74.
- [54] C. Albayrak, N. Ozkan, O. Dag, *Langmuir* 27 (2011) 870–873.
- [55] G.J. de A.A. Soler-Illia, C. Sanchez, *New J. Chem.* 24 (2000) 493–499.
- [56] C. Albayrak, A. Cihaner, O. Dag, *Chem. Eur. J* 18 (2012) 4190–4194.
- [57] A.A. Ismail, D.W. Bahnemann, L. Robben, V. Yarovsky, M. Wark, *Chem. Mater.* 22 (2010) 108–116.
- [58] G.-Q. Qu, *Spectrochim. Acta, Part A* 68 (2007) 905–907.
- [59] Z.V. Saponjic, N.M. Dimitrijevic, O.G. Poluektov, L.X. Chen, E. Wasinger, U. Welp, D.M. Tiede, X. Zuo, T. Rajh, *J. Phys. Chem. B*, 110 (2006) 25441–25450.
- [60] M.I. Zaki, M.A. Hasan, L. Pasupulety, K. Kumari, *New J. Chem.* 22 (1998) 875–882.
- [61] A.L. Shugarman, *Dissertation of California Institute of Technology, Autoxidation of manganese(II) β diketonate, Pasadena, US, 1968.*
- [62] A. Dassler, A. Feltz, J. Jung, W. Ludwig, E. Kaisersberger, *J. Therm. Anal* 33 (1988) 803–809.
- [63] K.S.W. Sing, *Pure Appl. Chem.* 54 (1982) 2201–2218; M. Thommes, *Chem. Ing. Tech.* 82 (2010) 1059–1073.
- [64] J. Ye, W. Liu, J. Cai, S. Chen, X. Zhao, H. Zhou, L. Qi, *J. Am. Chem. Soc.* 133 (2011) 933–940.
- [65] B. Choudhury, A. Choudhury, *Curr. Appl. Phys.* 13 (2013) 1025–1031.
- [66] Q. Tanga, X. Huang, Y. Chen, T. Liu, Y. Yang, *J. Mol. Catal. A: Chem* 301 (2009) 24–30.
- [67] H. Kaftelen, M. Tuncer, S. Tu, S. Repp, H. Goçmez, R. Thomann, S. Weber, E. Erdem, *J. Mater. Chem. A* 1 (2013) 9973.
- [68] K.C. Heo, C.I. Ok, J.W. Kim, *J. Korean Phys. Soc.* 47 (2005) 861–865.
- [69] M. Ramstedt, *Chemical Processes at the Water–Manganite (γ -MnOOH) Interface*, Dissertation Umea University, 2004.
- [70] H. Li, D. Wang, H. Fan, T. Jiang, X. Li, T. Xie, *Nano Res* 4 (2011) 460–469.
- [71] L. Zhang, D. He, P. Jiang, *Catal. Commun* 10 (2009) 1414–1416.
- [72] N. Nishimura, J. Tanikawa, M. Fujii, T. Kawahara, J. Ino, T. Akita, T. Fujino, H. Tada, *Chem. Commun* (2008) 3564–3566.
- [73] B. Ammundsen, G.R. Burns, D.J. Jones, J. Rozière, *J. Sol–Gel Sci. Technol* 8 (1997) 331–336.
- [74] B. Ammundsen, D.J. Jones, J. Rozière, G.R. Burns, *Chem. Mater.* 9 (1997) 3236–3246.
- [75] H.S. Lee, W.H. Kim, J.H. Lee, D.J. Choi, Y.-K. Jeong, J.H. Chang, *J. Solid State Chem* 185 (2012) 89–94.